Supporting Information

Circumferential lithium metal deposition at high rate enabled by synergistic effect of lithiophilic and ionic conductive network

Nan Zheng[a,b,c], Chao Liang[b], Cong Wu[b], Xun Zhang[b], Wenbo Zhai[b], MingXian Liu[a], Hengsheng Wei[a], Chang Zhang[b], Lei Dong[b], Yi Yu[b], Wei Liu[b], Lei Yao[a,*]

a Shenzhen Key Laboratory of Special Functional Materials, Shenzhen Engineering Laboratory for Advanced Technology of Ceramics, Guangdong Research Center for Interfacial Engineering of Functional Materials, College of Materials Science and Engineering, Shenzhen University, Shenzhen 518060, P. R. China

b School of Physical Science and Technology, ShanghaiTech University, Shanghai 201210, China

c Hanshan Normal University, Chaozhou 521041, China

∗ Corresponding Author:

E-mail address: lyao@szu.edu.cn (Lei Yao).

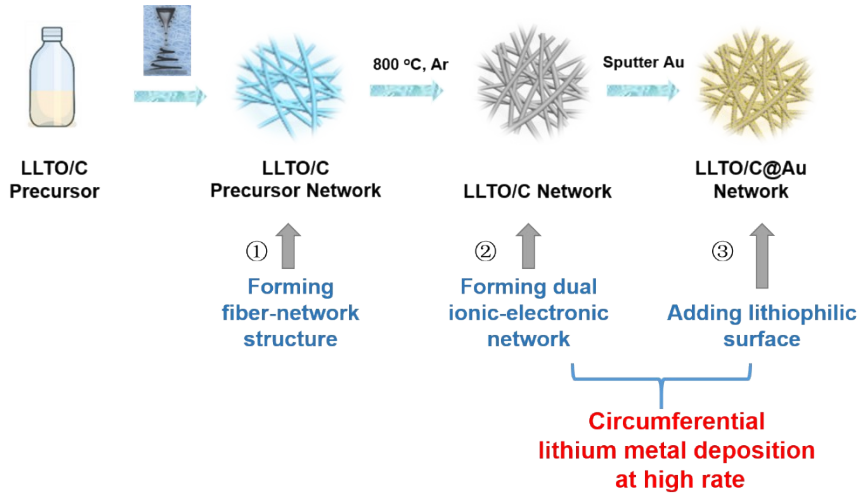

Fig. S1 Schematic illustration of the fabrication procedures and the intention of every procedure of LLTO/C@Au network.

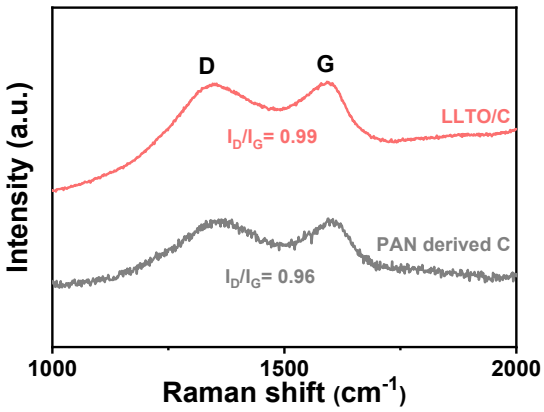

Fig. S2 The Raman spectra of LLTO/C and PAN derived carbon.

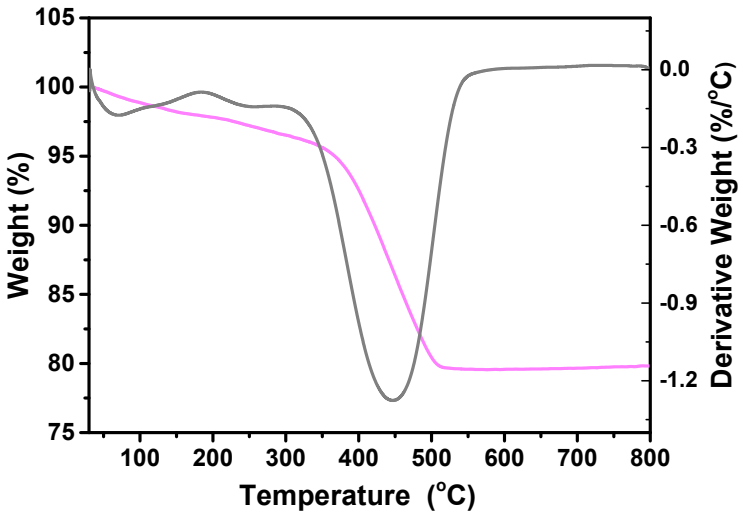

Fig. S3 TG and DTG curves of LLTO/C NWs.

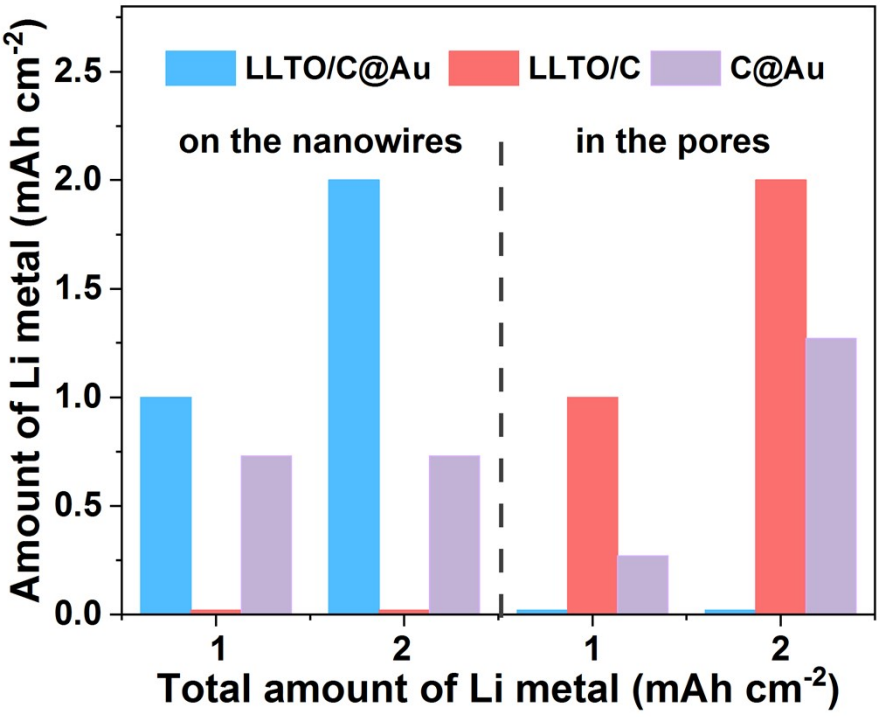

Fig. S4 The amount of Li metal distribution in these 3D host after Li plating in the Fig. 3.

Calculation of the content distributions of the Li-metal deposition in these 3D host

The area of 12 mm electrode is 1.13 cm^2

Plating 1 mAh cm^{-2} Li metal, the capacity of Li is 1.13 mAh，

m_{Li} = 1.13/3860 g = 0.293 mg, $V_{Li1} = m_{Li}/\rho_{Li}$ = 0.293/534 cm^3 = 5.49*10^{-4} cm^3

Plating 2 mAh cm^{-2} Li metal, V_{Li2} = 5.49*2*10^{-4} cm^3 = 1.1*10^{-3} cm^3

Specific surface area: $S_{LLTO/C} \approx S_{LLTO/C@Au}$; $S_C \approx S_{C@Au}$;

For LLTO/C@Au

Plating 1 mAh cm^{-2} Li metal

The mass of 12 mm electrode is 8.4 mg, $S_{electrode}$ = 3.7*8.8*10^{-3} m^2 = 3.26*10^{-2} m^2 ,

The plating thickness of Li metal on the LLTO/C@Au NWs:

ΔL = 5.49*10^{-4} cm^3/ 3.26*10^{-2} m^2 ≈1.68*10^{-6} cm = 16.8 nm

Plating 2 mAh cm−2 Li metal

ΔL = 16.8 nm*2 = 33.6 nm

For C@Au

Plating 1 mAh cm^{-2} Li metal,

It is assumed that the thickness of Li deposition is only half of C@Au membrane.

If all Li metal is plated on the C@Au NWs,

The mass of 12 mm electrode is 1.3 mg,

The area of Li metal deposition on the C@Au NWs:

$S_{electrode}$ = 1.3*26.9*10^{-3} *1/2= 1.75*10^{-2} m^2 ,

The plating thickness of Li metal on the C@Au NWs:

ΔL = 5.49*10^{-4} cm^3/ 1.75*10^{-2} m^2 ≈3.14*10^{-6} cm = 31.4 nm ,

But as shown in the Fig. 3D, part of Li metal deposited between the C@Au NWs. It is assumed that this part of lithium accounts for 23% of the total lithium.

So the capacity of Li deposited between the C@Au NWs is 0.23 mAh cm^{-2} ,

The capacity of Li deposited between the C@Au NWs:

1-0.23= 0.73 mAh cm^{-2}

The actual plating thickness of Li metal on the C@Au NWs:

$\Delta L = 31.4 * 0.73\ nm = 22.9\ nm$

Plating 2 mAh cm^{-2} Li metal,

the capacity of Li deposited between the C@Au NWs is 0.23 mAh cm^{-2} ,

The capacity of Li deposited on the C@Au NWs:

2-0.73=1.27 mAh cm^{-2}

For LLTO/C

Li metal nearly cannot be plated on the surface of LLTO/C NWs due to its lithiophobic surface.

So plating 1 mAh cm^{-2} Li metal,

the capacity of Li deposited between the LLTO/C NWs is 1 mAh cm^{-2},

plating 2 mAh cm^{-2} Li metal,

the capacity of Li deposited between the LLTO/C NWs is 2 mAh cm^{-2}.

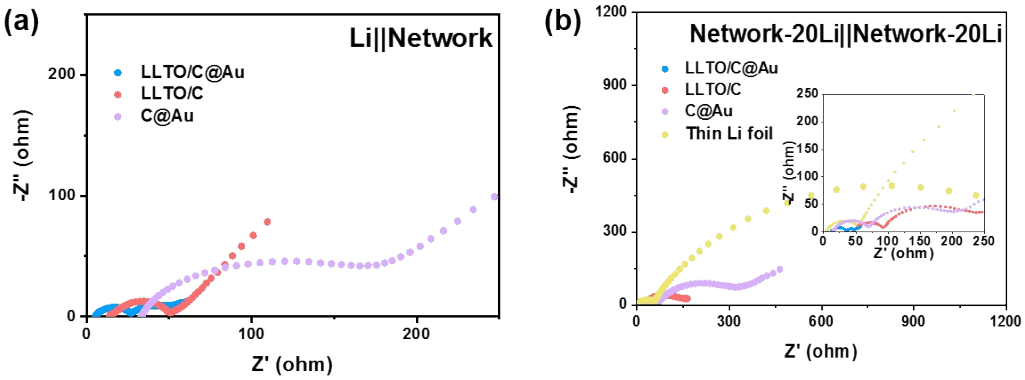

Fig. S5 (a) Nyquist plots of Li||Host cells with no Li metal on host. (b) Nyquist plots of Host−20Li||Host−20Li cells with plating 20 mAh cm^{-2} Li metal on host and thin Li foil||thin Li foil.

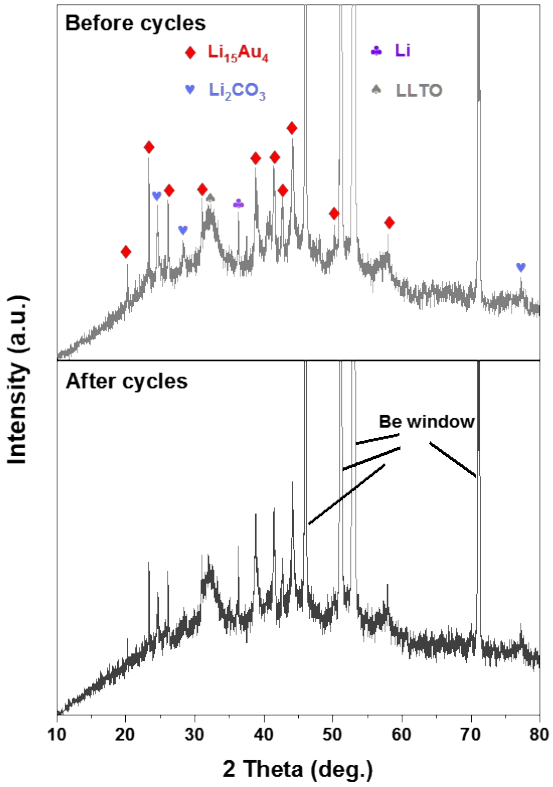

Fig. S6 The *ex-situ* XRD patterns of LLTO/C@Au-Li anode before and after cycling.

In order to better detect the signals of Au–Li alloy, only 5 mAh cm^{-2} of Li metal were deposited in LLTO/C@Au network. *Ex-situ* XRD tests were carried out for LLTO/C@Au-Li electrode before and after 50 cycles at 3 mA cm^{-2}/1 mAh cm^{-2} (symmetrical batteries). The results (**Fig. S6**) show that the XRD peaks of Au–Li alloy ($Li_{15}Au_4$) hardly change [1], confirming the existence of Au-Li alloy during the cycling. This is because the Au-Li alloy exists at the bottom of Li metal. If the high-capacity battery cycling is not carried out, the Au-Li alloy does not participate in the reaction during the cycling process, but plays a role in the initial nucleation process, and only the Li metal on the surface participates in the battery cycling.

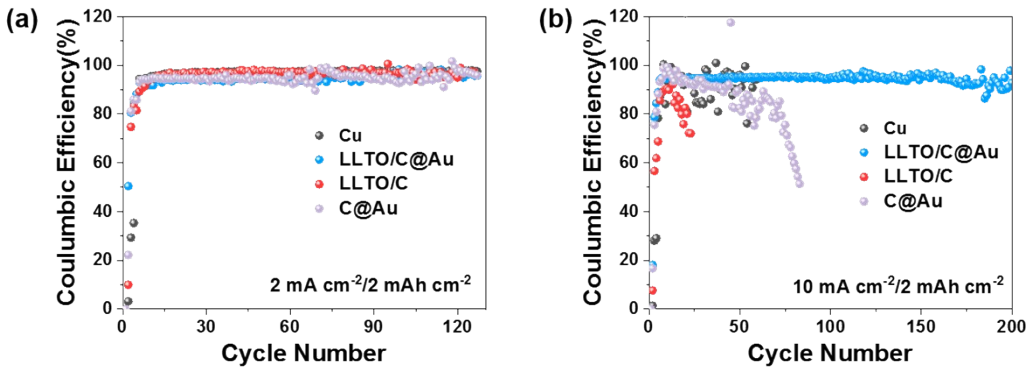

Fig. S7 Coulombic efficiency of the Li stripping/platting cycles of the three hosts in comparison with Cu foil at current densities of (a) 2 mA cm^{-2} and (b) 10 mA cm^{-2} with a capacity of 2 mAh cm^{-2}.

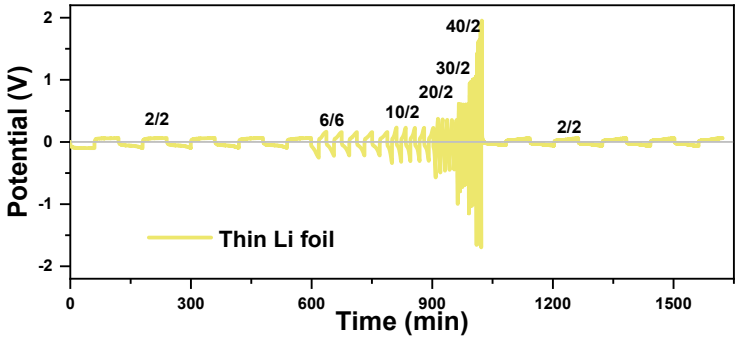

Fig. S8 Rate performances of Thin Li foil symmetrical cell with a capacity of 2 mAh cm^{-2} (the unit for each current is mA cm^{-2}/mAh cm^{-2}).

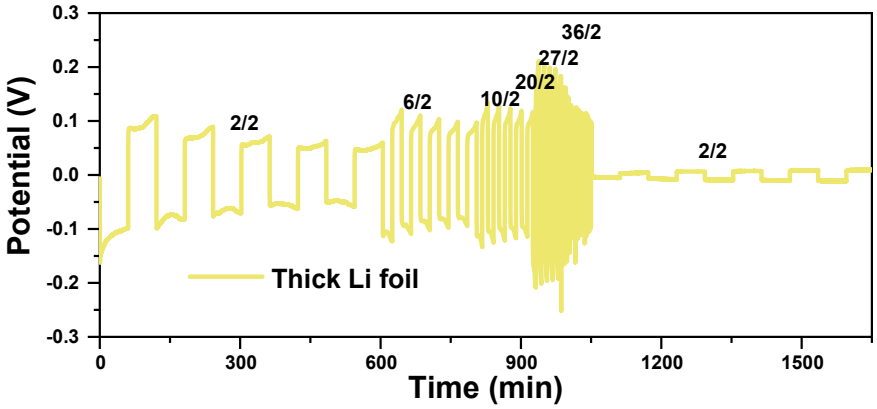

Fig. S9 The rate performance of Thick Li foil symmetrical cell with a capacity of 2 mAh cm^{-2} (the unit for each current is mA cm^{-2}/mAh cm^{-2}).

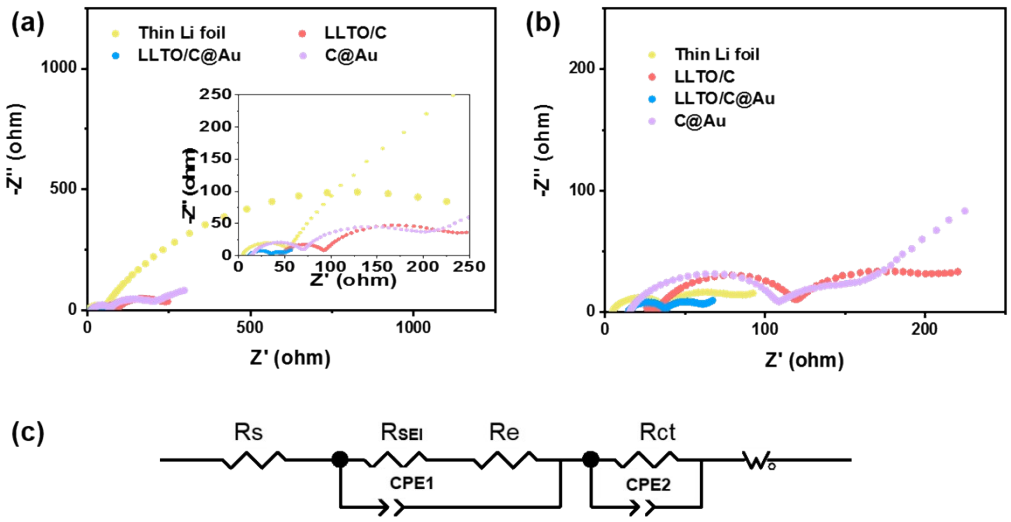

Fig. S10 Nyquist plots of the symmetric cells (a) at fresh state and (b) after 10th cycles at 10 mA cm^{-2}/2 mAh cm^{-2}, respectively. (c) Equivalent circuit used for Nyquist plots of the symmetric cells.

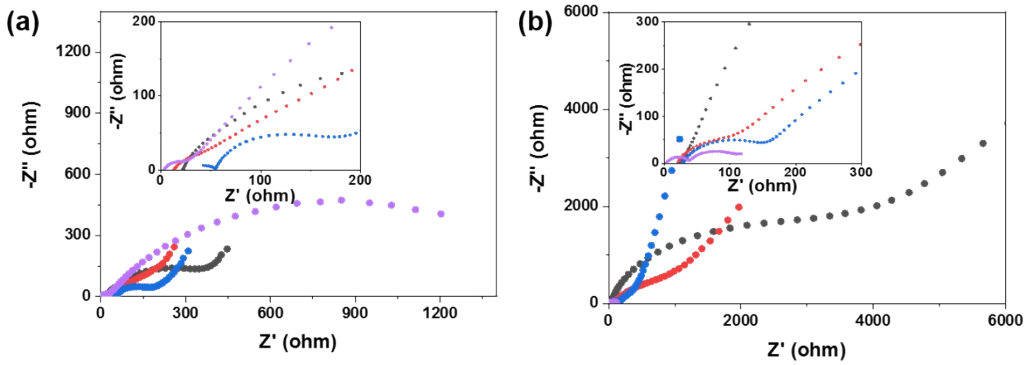

Fig. S11 Nyquist plots of the full cells in the (a) fresh state and (b) after rate cycles, respectively.

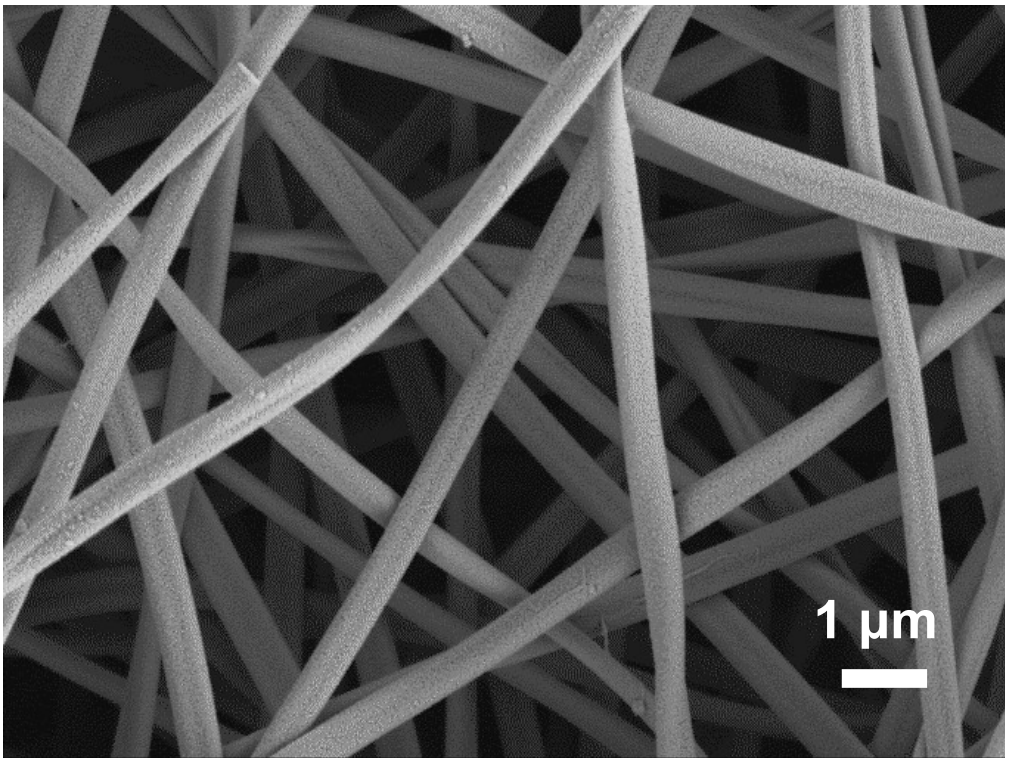

Fig. S12 SEM image of LLTO/C@Au NWs.

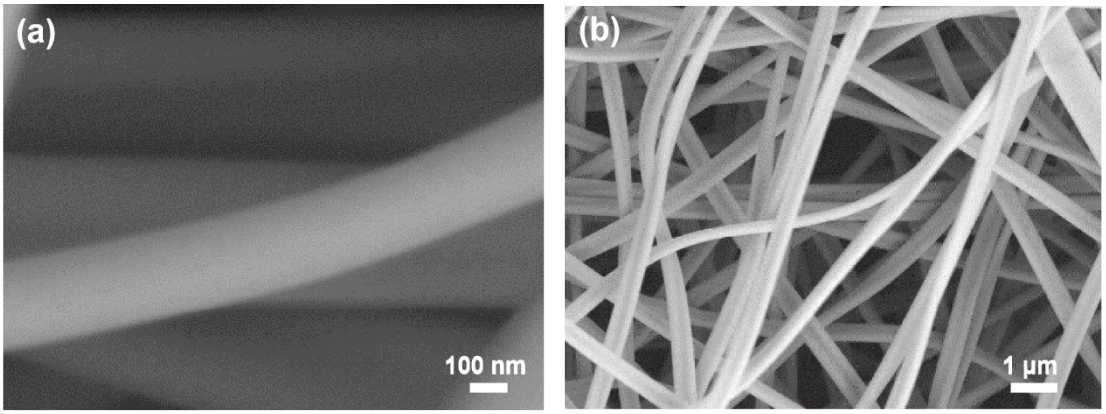

Fig. S13 (a-b) SEM images of LLTO/C NWs.

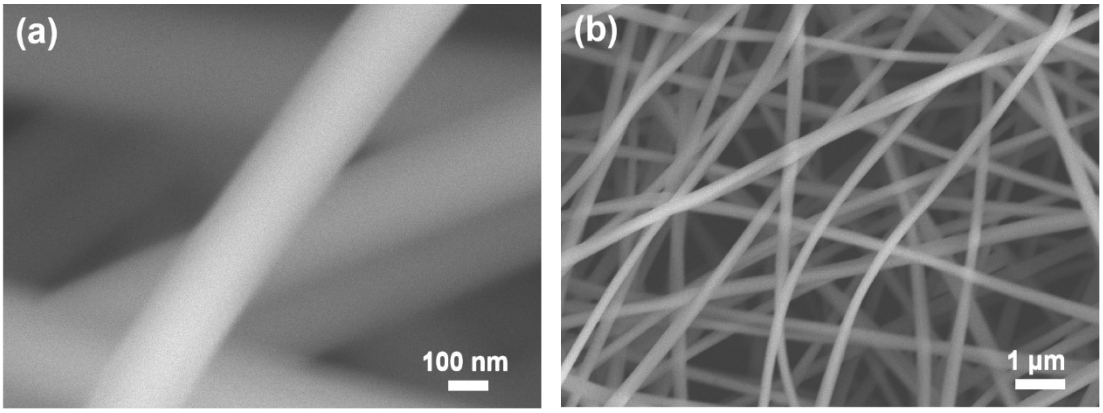

Fig. S14 (a-b) SEM images of C NWs.

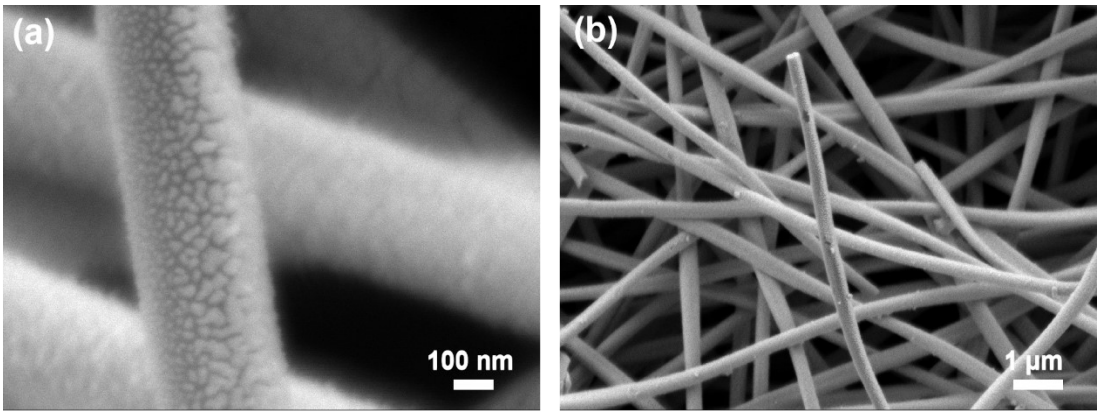

Fig. S15 (a-b) SEM images of C@Au NWs.

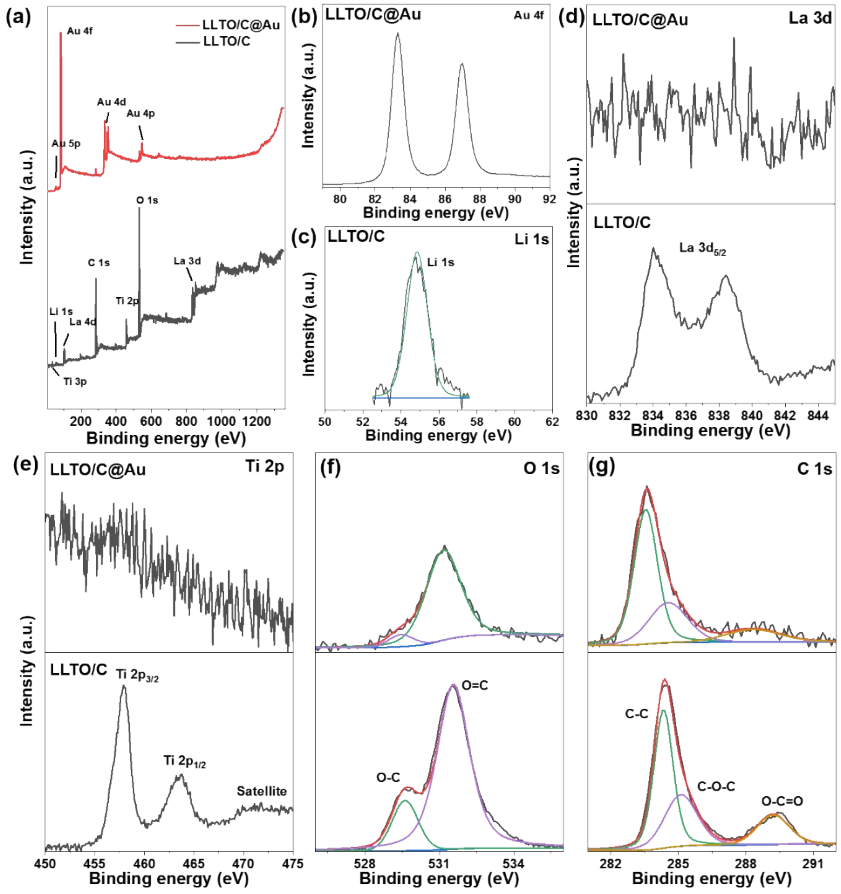

Fig. S16 Comparison of XPS spectra of the LLTO/C@Au and LLTO/C. (a) XPS survey scans. (b) XPS spectrum of Au 4f in the LLTO/C@Au. (c) XPS spectrum of Li 1s in the LLTO/C. XPS spectra comparisons of (d) La 3d, (e) Ti 2p, (f) O 1s and (g) C 1s.

From the XPS analysis (**Fig. S16** and **Table S6**), it is revealed that the surface of LLTO/C@Au is mainly composed of Au (91.7 wt%), which is much different from that of LLTO/C.

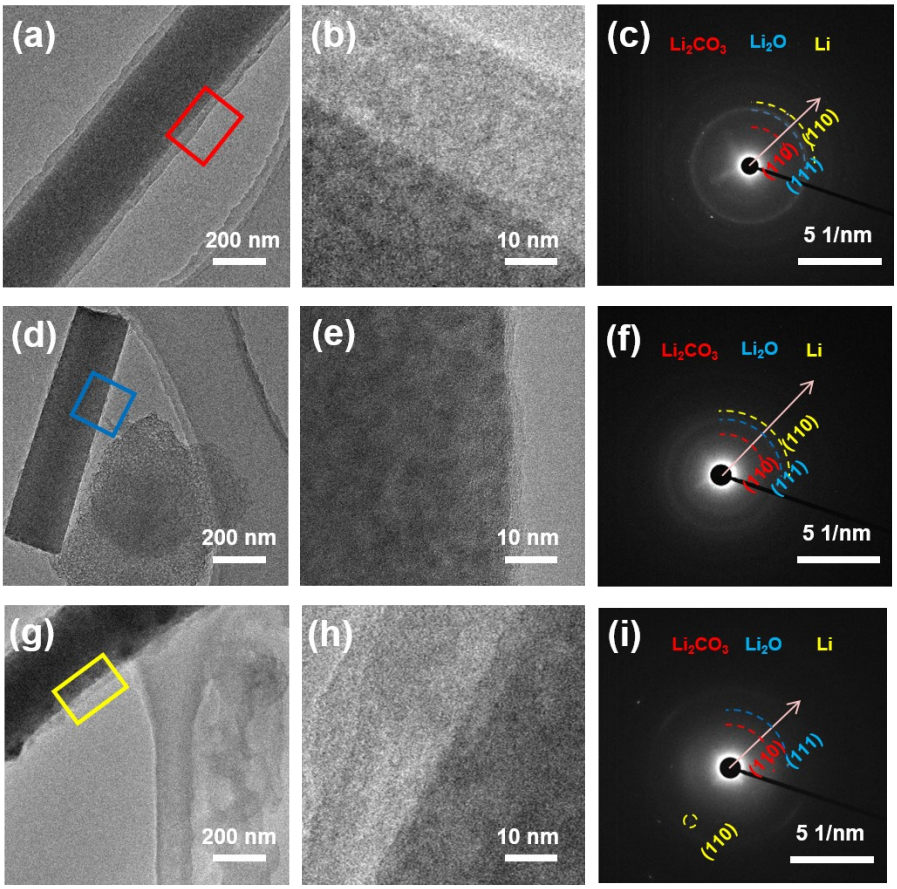

Fig. S17 The TEM images and SAED images of the different anodes after cycling. (a-c) LLTO/C@Au-Li anode. (d-f) LLTO/C-Li anode. (g-i) C@Au-Li anode.

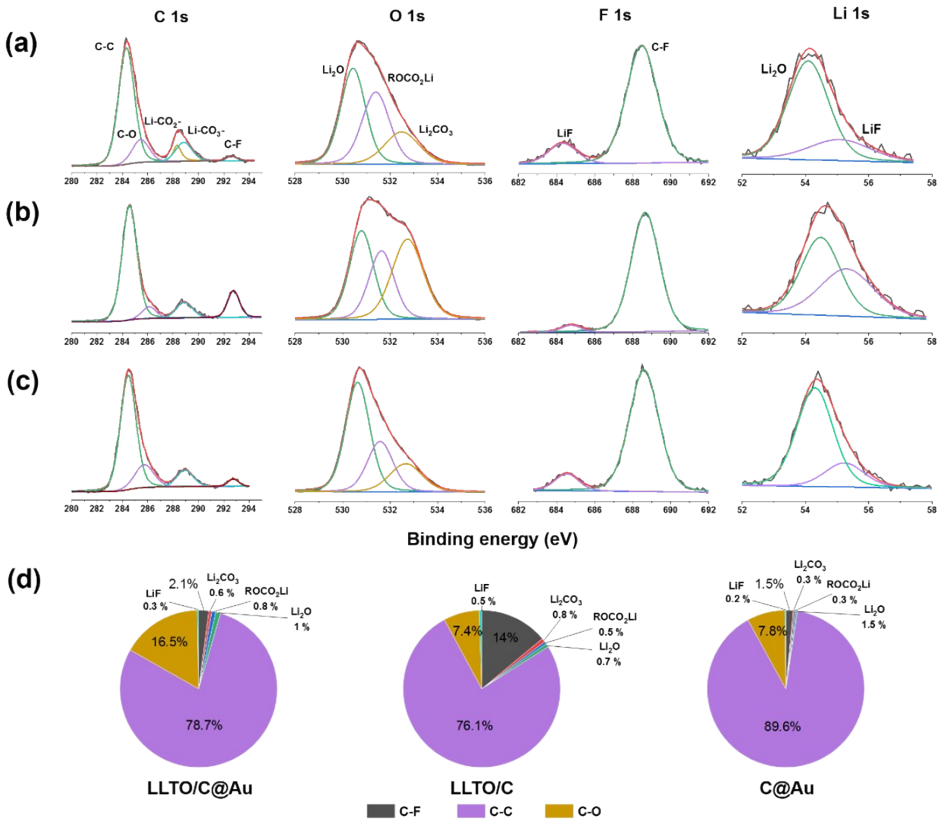

Fig. S18 Composition of Li metal SEI in different anodes after cycling. (a) XPS spectra of the Li SEI in LLTO/C@Au-Li anode. (b) XPS spectra of the Li SEI in LLTO/C-Li anode. (c) XPS spectra of the Li SEI in C@Au-Li anode. (d) Quantification of surface compositions of Li metal SEI obtained by XPS data.

The morphology and components of SEI in different anodes after cycling were confirmed by TEM and XPS characterizations. Only 2 mAh cm^{-2} of Li metal were deposited in these networks to facilitate detection. After 25 cycles at 2 mA cm^{-2}/1 mAh cm^{-2}, these symmetrical batteries used by these Network-Li electrodes were disassembled for analysis. It can be seen from the TEM images (**Fig. S17**) that Li metal is still uniformly attached to the surface of LLTO/C@Au network, while Li

metal can hardly be deposited on the surface of LLTO/C network and can only be partially deposited on the surface of C@Au network after cycling. The Li_2CO_3 and Li_2O in the SEI of these electrodes can all be confirmed by the SAED images. Various trace organic and inorganic components on the surface of SEI in different anodes after cycling were further detected by the XPS tests. In XPS analysis (**Fig. S18**), the C-F and LiF in the SEI surface of LLTO/C-Li anode are significantly more than that of LLTO/C@Au-Li anode and C@Au-Li anode, indicating that its SEI is unstable, which continuously consumes electrolyte during cycling.[2, 3] There are more organic components C-C in the SEI surface of C@Au-Li anode because of larger specific surface area of C@Au network (**Fig. S22**) and the partial Li metal deposited on the surface of C@Au NWs. As a result, the SEI of LLTO/C@Au-Li electrode exhibits the best stability among the three electrodes during cycling according to TEM images and XPS analysis.

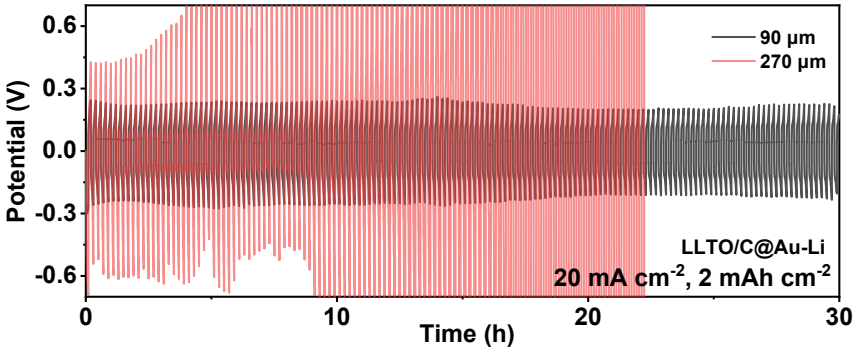

Fig. S19 Comparison of the voltage profiles obtained during Li plating/stripping at 20 mA cm^{-2}/2 mAh cm^{-2} for LLTO/C@Au-Li half cells with different thicknesses of the LLTO/C@Au network films.

The influence of the thickness of the network film on the electrochemical properties of the battery has been investigated. It is revealed that the internal resistance of the electrode increases with the thickness of the network films, which in turns decreases the electron transfer rate, increases the polarization of the battery and reduces the cycle life of the battery. **Fig. S19** shows the voltage profiles obtained during Li plating/stripping at 20 mA cm^{-2}/2 mAh cm^{-2} for LLTO/C@Au-Li half cells with different thicknesses of the LLTO/C@Au. As can be seen, the polarization of the batteries increases and the cycle life of the batteries decreases significantly as the thickness of the LLTO/C@Au film increases by three times. In contrast, the mechanical strength of the network film increases with the thickness. Therefore, the thickness of the network film used in this work has been carefully optimized as ~90 μm.

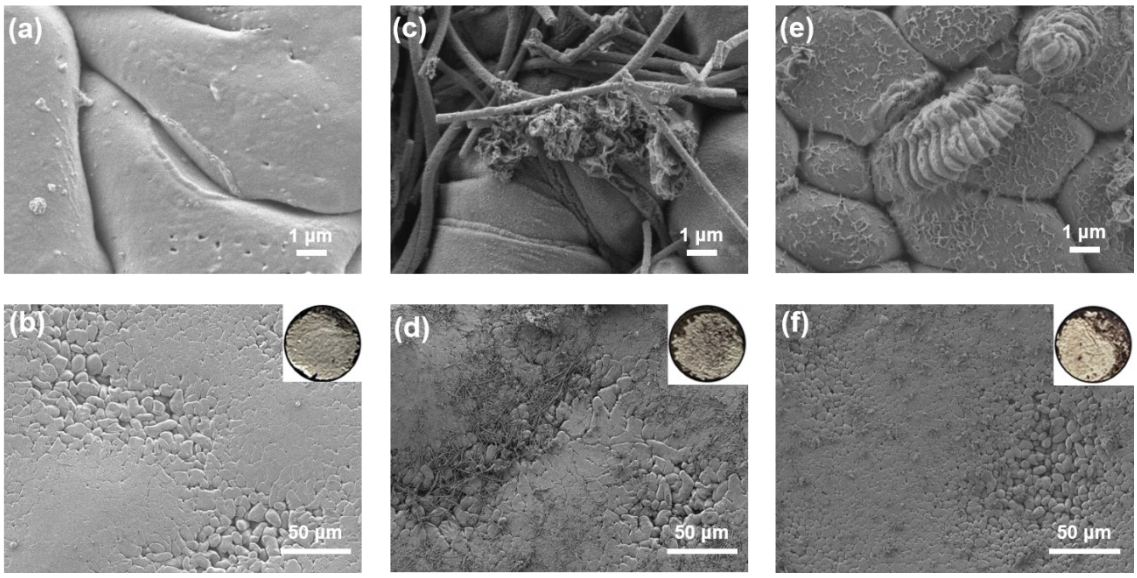

Fig. S20 The SEM images and optical photographs of the different anodes after cycling. (a-b) The SEM images of LLTO/C@Au-Li anode. The inset in (b) is the optical photograph of LLTO/C@Au-Li anode. (c-d) The SEM images of LLTO/C-Li anode. The inset in (d) is the optical photograph of LLTO/C-Li anode. (e-f) The SEM images of C@Au-Li anode. The inset in (f) is the optical photograph of C@Au-Li anode.

The surface morphologies of Li metal in different networks after 50 cycles at 20 mA cm^{-2}/2 mAh cm^{-2} (symmetrical batteries) were investigated by *ex situ* SEM. As shown in **Fig. S20**, Li metal is mainly deposited in the form of compact particles in all three networks. However, LLTO/C network is partially exposed on the surface of the deposited Li metal, and some "dead Li" exists in the LLTO/C network (**Fig. S20c-d**) and some mossy Li metal exists in C@Au network (**Fig. S20e-f**). The optical photographs (the inset in **Fig. S20b, d and f**) are consistent with the corresponding SEM images. It indicates that the three networks all have a certain inhibitory effect on

the formation of Li dendrites. LLTO/C@Au network has more advantages for cycling at the high current and high capacity, and almost no dead Li or other forms of Li dendrites can be observed in it (**Fig. S20a-b**).

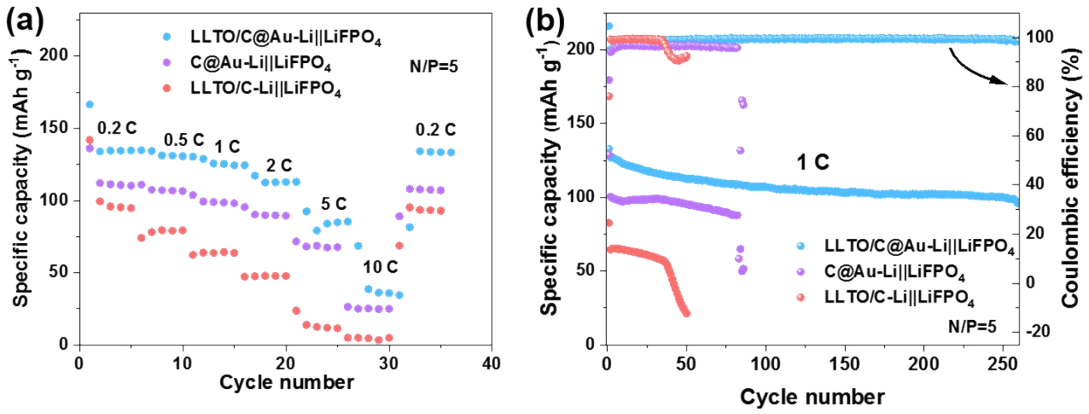

Fig. S21 Comparison of the performance of full cells paired with the different anodes. (a) The rate performance comparisons. (b) The cycling performance comparisons at 1 C.

As illustrated in **Fig. S21**, the performance of the full cell paired with LLTO/C@Au anode is obviously better than that of other full cells. During cycling at 1C, the capacities of full cells paired with C@Au and LLTO/C anodes decay rapidly after 83 cycles and 37 cycles, respectively, while that of full cell paired with LLTO/C@Au still exhibits a capacity of 96 mAh g^{-1} after 260 cycles.

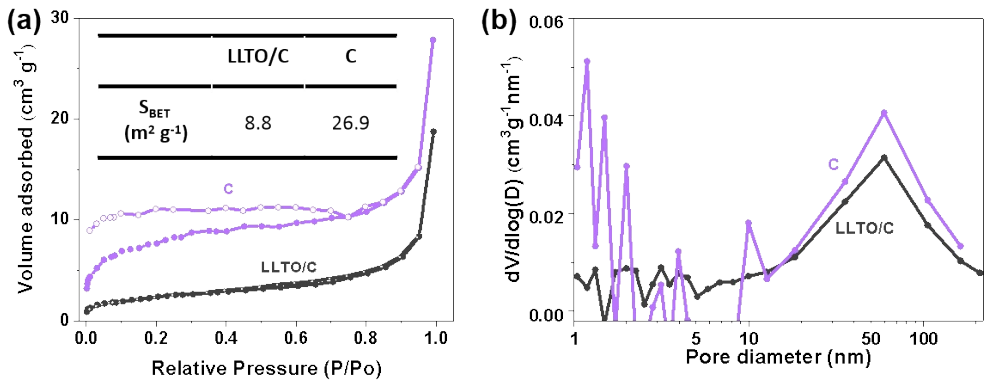

Fig. S22 (a) N_2 adsorption–desorption isotherms and (b) pore size distribution curves of LLTO/C NWs and C NWs. The inset is specific surface area data of these two materials.

Table S1 The accommodated Li metal capacity of three host

	Density ($g\ cm^{-3}$)	Average Porosity	Thickness (μm)	Mass ($mg\ cm^{-2}$)	Pore volume ($cm^3\ g^{-1}$)	Accommodated Li capacity ($mAh\ cm^{-2}$)	Weight ratio of Li metal
LLTO/C@Au	2.86	75 %	~ 90	3.27	1.05	13.9	0.36
LLTO/C	2.47	77 %	~ 90	3.01	1.36	14.3	0.42
C@Au	1.56	86 %	~ 90	1.15	3.94	15.9	0.68

Table S2 The comparisons of cycling life between the as-prepared LLTO/C@Au–Li anode and the other reported typical composite 3D Li anode at high current density and high capacity

Configuration	Li infiltration method	Symmetric cell (mA cm^{-2}/mAh cm^{-2})	Electrolyte	Ref.
The spaced TiO_2 NTs	Thermal infusion	4.0/4.0, 450 h voltage ≈ 50 mV	1 M LiTFSI in DOL:DME (1:1) with 2 wt% $LiNO_3$	4
3D Cu NWs	Electrodeposition	1.0/2.0, 500 h voltage ≈ 20 mV	1 M LiTFSI in DOL:DME (1:1) with 1 wt% $LiNO_3$ + 5 × 10^{-3} M Li_2S_8	5
MWCNTs	Mechanical lamination	10.0/5.0, 180 h voltage ≈ 70 mV	1 M LiTFSI in DOL:DME (1:1)	6
C@ ZnO	Thermal infusion	10.0/5.0, 300 h voltage ≈ 90 mV	1 M $LiPF_6$ in EC:EMC:DEC (1:1:1)	7
LLZO/C	Electrodeposition	5.0/1.0,650 h voltage ≈ 40 mV	1 M LiTFSI in DOL:DME (1:1) with 1 wt% $LiNO_3$	8
3D VACNF/Cu	Electrodeposition	5.0/5.0, 185 h voltage ≈ 35 mV	1 M LiTFSI in DOL:DME (1:1) with 1 wt% $LiNO_3$	9
Cu mesh	Thermal infusion	1.0/6.0, 600 h voltage ≈ 30 mV	1 M LiTFSI in DOL:DME (1:1) with 1 wt% $LiNO_3$	10
This work (LLTO/C@Au)	Electrodeposition	2.0/10.0, 500 h voltage ≈ 50 mV	1 M LiTFSI in DOL:DME (1:1) with 1 wt% $LiNO_3$	-

Table S3 Impedance parameters obtained from EIS spectra in Fig. S10a-b

Sample	Fresh state				After cycles			
	Rs (Ω)	**R_{SEI}+Re (Ω)**	**Rct (Ω)**	**R_{total} (Ω)**	**Rs (Ω)**	**R_{SEI}+Re (Ω)**	**Rct (Ω)**	**R_{total} (Ω)**
Thin Li foil	4.3	54.7	1409.6	1468.6	4.5	34.3	44.9	83.7
LLTO/C NWs	44.9	50.4	164.6	259.9	32.3	91.1	96.3	219.7
LLTO/C@Au NWs	10.8	24.9	16.3	52.0	14.4	24.7	30.1	69.2
C@Au NWs	14.1	59.4	159.3	232.8	15.6	96.3	74.2	186.1

Table S4 Impedance parameters obtained from EIS spectra in Fig. S11a-b

Sample	Fresh state				After cycles			
	Rs (Ω)	R_{SEI}+Re (Ω)	Rct/R_{SEI}+Re + Rct(Ω)	Rtotal (Ω)	Rs (Ω)	R_{SEI}+Re (Ω)	Rct/R_{SEI} +Re+ Rct(Ω)	Rtotal (Ω)
N/P 1.5 (LLTO/C@Au @Li)	22.4	-	445.8	468.2	26.8	-	5605.7	5632.5
N/P 3 (LLTO/C@Au @Li)	14.9	43.2	244.1	302.2	19.6	-	146.9	166.5
N/P 5 (LLTO/C@Au @Li)	32.5	21.5	161.4	215.4	23.2	-	151.6	174.8
N/P 12 (Thin Li foil)	4.2	29.0	1473.7	1506.9	3.9	33	77.6	114.5

Table S5 The full cell performances comparison with Li metal as anodes

Materials	Cathode	N/P	Current Density(C)	Cycle number	Reference
LLZO/C	$LiFePO_4$	2	0.5	100	[8]
Co@N-G	$LiNi_{0.5}Co_{0.2}Mn_{0.3}O_2$ (NCM)	-	1	100	[11]
CFs@Au	S	1.2	0.1	100	[12]
single-ion electrolyte	$LiFePO_4$	-	1	2000	[13]
Li_3N@Cu NWs–Li	LCO	-	0.5	300	[14]
EC-ES electrolyte	$LiFePO_4$	31	1	300	[15]
Polymer–Alloy Hybrid Layers	$LiFePO_4$	34	0.5	300	[16]
Polydopamine /Graphene Layer	$LiFePO_4$	-	1	1000	[17]
C–N film	$LiFePO_4$	1.5	0.5	65	[18]
Coaxial-interweaved hybrid Li metal anode	$LiFePO_4$	7.9	1	135	[19]
LLTO/C@Au	$LiFePO_4$	3 5	0.5	86 370	This work

Table S6 Quantification of the samples obtained by XPS data in Fig. S16

Sample	Li (wt%)	La (wt%)	Ti (wt%)	O (wt%)	C (wt%)	Au (wt%)
LLTO/C@Au	-	-	-	3.3	5.0	91.7
LLTO/C	5.9	10.0	12.0	32.7	39.4	-

References

1 T. Yang, Y. Li, C. K. Chan, *J. Power Sources,* 2015, **287**, 164-169.

2 D. Lin, Y. Liu, Y. Li, Y. Li, A. Pei, J. Xie, W. Huang, Y. Cui, *Nat. Chem.,* 2019, **11**, 382-389.

3 H. Kwon, J.-H. Lee, Y. Roh, J. Baek, D. J. Shin, J. K. Yoon, H. J. Ha, J. Y. Kim, H.-T. Kim, *Nat. Commun.,* 2021, **12**, 5537.

4 K. Tantratian, D. Cao, A. Abdelaziz, X. Sun, J. Sheng, A. Natan, L. Chen, H. Zhu, *Adv. Energy Mater.,* 2020, **10**, 1902819.

5 L.-L. Lu, J. Ge, J.-N. Yang, S.-M. Chen, H.-B. Yao, F. Zhou, S.-H. Yu, *Nano Lett.,* 2016, **16**, 4431-4437.

6 Y. Deng, H. Lu, Y. Cao, B. Xu, Q. Hong, W. Cai, W. Yang, *J. Power Sources,* 2019, **412**, 170-179.

7 X. Wang, Z. Pan, Y. Wu, X. Ding, X. Hong, G. Xu, M. Liu, Y. Zhang, W. Li, *Nano Res.,* 2019, **12**, 525-529.

8 C. Zhang, S. Liu, G. Li, C. Zhang, X. Liu, J. Luo, *Adv. Mater.,* 2018, **30**, 1801328.

9 Y. Chen, A. Elangovan, D. Zeng, Y. Zhang, H. Ke, J. Li, Y. Sun, H. Cheng, *Adv. Funct. Mater.,* 2020, **30**, 1906444.

10 S. Huang, L. Chen, T. Wang, J. Hu, Q. Zhang, H. Zhang, C. Nan, L.-Z. Fan, *Nano Lett.,* 2021, **21**, 791-797.

11 T.-S. Wang, X. Liu, X. Zhao, P. He, C.-W. Nan, L.-Z. Fan, *Adv. Funct. Mater.,* 2020, **30**, 2000786.

12 J. Xiang, L. Yuan, Y. Shen, Z. Cheng, K. Yuan, Z. Guo, Y. Zhang, X. Chen, Y. Huang, *Adv. Energy Mater.,* 2018, **8**, 1802352.

13 S. Yuan, J. L. Bao, J. Wei, Y. Xia, D. G. Truhlar, Y. Wang, *Energy Environ. Sci.,* 2019, **12**, 2741-2750.

14 D. Lee, S. Sun, J. Kwon, H. Park, M. Jang, E. Park, B. Son, Y. Jung, T. Song, U. Paik, *Adv. Mater.,* 2020, **32**, 1905573.

15 Y. Zhang, Y. Zhong, Z. Wu, B. Wang, S. Liang, H. Wang, *Angew. Chem., Int. Ed.,* 2020, **59**, 7797-7802.

16 Z. Jiang, L. Jin, Z. Han, W. Hu, Z. Zeng, Y. Sun, J. Xie, *Angew. Chem., Int. Ed.,* 2019, **58**, 11374-11378.

17 P. J. Kim, V. G. Pol, *Adv. Energy Mater.,* 2018, **8**, 1802665.

18 Q. Yang, M. Cui, J. Hu, F. Chu, Y. Zheng, J. Liu, C. Li, *ACS Nano,* 2020, **14**, 1866-1878.

19 X.-R. Chen, B.-Q. Li, C. Zhu, R. Zhang, X.-B. Cheng, J.-Q. Huang, Q. Zhang, *Adv. Energy Mater.,* 2019, **9**, 1901932.